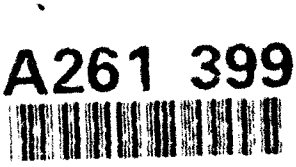

(2)

THE OHIO STATE UNIVERSITY

IR and FIR Laser Diagnostics For Plasma Thrusters Using a CW CO_2 Radiation Source

Thomas M. York
Department of Aeronautical and Astronautical Engineering

Air Force Office of Scientific Research
Bolling Air Force Base, D.C. 20332

Grant No. AFOSR-91-0201
Final Report

November 1992

REPORT DOCUMENTATION PAGE

Form Approved
OMB No 0704-0188

1. AGENCY USE ONLY (Leave blank)	2. REPORT DATE	3. REPORT TYPE AND DATES COVERED
	30 Nov 1992	Final

4. TITLE AND SUBTITLE

IR and FIR Laser Diagnostics for Plasma Thrusters Using a CW CO_2 Radiation Source

5. FUNDING NUMBERS

AFOSR-91-0201

6. AUTHOR(S)

Thomas M. York

7. PERFORMING ORGANIZATION NAME(S) AND ADDRESS(ES)

Ohio State University Research Foundation
1960 Kenny Rd.
Columbus, Ohio 43210

NA

8. PERFORMING ORGANIZATION REPORT NUMBER

RF 768960/724586

9. SPONSORING/MONITORING AGENCY NAME(S) AND ADDRESS(ES)

AFOSR/XPT
110 Duncan Ave, Suite B115
BAFB DFB 20332-0001

10. SPONSORING/MONITORING AGENCY REPORT NUMBER

11. SUPPLEMENTARY NOTES

12a. DISTRIBUTION/AVAILABILITY STATEMENT

Approved for public release,
distribution unlimited

12b. DISTRIBUTION CODE

13. ABSTRACT *(Maximum 200 words)*

This research involves diagnostic studies of plasma thrusters. This effort will use the new, high resolution diagnostic techniques that will determine electron densities, local magnetic fields, and density fluctuations indicating anomalous transport.

14. SUBJECT TERMS	15. NUMBER OF PAGES
	52
	16. PRICE CODE

17. SECURITY CLASSIFICATION OF REPORT	18. SECURITY CLASSIFICATION OF THIS PAGE	19. SECURITY CLASSIFICATION OF ABSTRACT	20. LIMITATION OF ABSTRACT
U	U	U	

THE OHIO STATE UNIVERSITY

IR and FIR Laser Diagnostics For Plasma Thrusters Using a CW CO_2 Radiation Source

Thomas M. York
Department of Aeronautical and Astronautical Engineering

Air Force Office of Scientific Research
Bolling Air Force Base, D.C. 20332

Grant No. AFOSR-91-0201
Final Report
RF Project No. 768960/724586

November 1992

CONTENTS

SUMMARY

The program of work and the accomplishments during this contract were affected by a number of factors:

(1) the one-year delay in support resulted in the departure from Ohio State of the graduate Research Associate who had been working for two years on this and related projects. We had to begin from a total new start with Research Associates.

(2) the conduct of the research required the development of new switch components for the experiments; unbudgeted equipment costs used 25% of the funds

(3) unforseen difficulties with CO_2 detectors have not yet been resolved, and there is no workable detector system; the supplier, Electric-Optical Systems, Phoenixville PA has still not met original specifications, critical for operation.

The research work that has been carried out on the effects of applied field magnetic nozzles has been highly successful. The key findings are:

(1) the time required for nozzle field penetration of the thrust chamber is about 200 ms.

(2) with increased field penetration in the thrust chamber, there is increased power delivery to the gas.

(3) with increased power delivery to the gas, there is increased heating and thrust (momentum flux) in the propellent.

(4) alteration of the magnetic nozzle shape has strong effects on the acceleration of the propellent for thrust purposes.

In summary, the results indicate substantial improvement of arc and MPD arc performance over self-field or thermal thrusters and should be pursued further.

STATEMENT OF WORK

(Revised June 1991 following acceptance of proposal)

This research effort will be directed to the development of new diagnostic techniques and their application to plasma thruster devices of interest. This proposal requests support for operating funds so that equipment already provided can be development and used in existing experiments.

During the one-year period of requested funding, the work will focus on the following:

1. Studies of ¼-scale MPD with Variable Magnetic Nozzle Fields

   This effort will continue the work initiated under NASA's support which showed strong enhancement of thrust with applied fields. The research will focus on two effects:

   (1) since earlier studies had a 400μs nozzle field duration and so lacked penetration into the thrust chamber, the present work will develop switching components and power supply to create lifetimes of at least one second and will study the effects on acceleration;

   (2) since the plasma expansion is affected by magnetic nozzles, the nozzle contours will be changed so that positive control over the expansion can be studied.

2. Multi-Beam Interferometric Study of ¼ Scale MPD

   Following a demonstration of proof-of-principle with a single beam in a known experiment, the system will be enlarged to four beams and applied to the ¼ Scale thruster. Profiles of Ne(r) will developed and comprehensive Ne(r,z) as

a function of time will be developed for low and high power self-field discharges; this will be basic to study of similar discharges with variable applied magnetic nozzle fields.

3. Initiation of Study to Develop a System to Measure Electron Density Fluctuations with a CO_2 Laser System.

A detailed layout of components needed and the subsequent design of an operable system to determine, first, the amplitude of fluctuations. The physics of such fluctuations as they relate to transport, particularly the confinement and difference related to applied nozzle field lines in the expansion flow of the thruster will be studies. With limited equipment funds, the acquisition of components to allow development of fluctuation sensitive diagnostic will probable have to wait until a third contract year.

RESEARCH ACCOMPLISHMENTS

1. Study of 50 - 150 KW Arc and MPD Arc Thruster with Applied Field Magnetic Nozzle
(H. Kamhawi)

The primary objective of this research was to study the effects of magnetic nozzles on the acceleration of plasma flow inside the 1/4-scale arc and MPD arc thruster. This research effort is an extension of previous research efforts carried out by York, Zakrzwski, and Soulas[1]. In the earlier work, the magnetic field strength was generated by a pulse forming network with run times on the order of 400 μsec; these run times were not long enough to allow the magnetic field to penetrate into the inter-electrode region. To be able to further study the effects of applied magnetic fields, the magnetic field penetration times and magnetic field nozzle shape were to be changed. This research examined the effects of magnetic field penetration into the discharge chamber on the performance and physical processes occurring in the 1/4-scale MPD thruster. Also, and equally important, this investigation analyzed the effects of changing the magnetic field line shapes (contours) on the overall performance of the thruster system. This was done by examining thruster operating parameters and plasma properties within the plume of the 1/4-scale MPD thruster operating at different current levels, with different magnetic field penetration times and different magnetic nozzle shapes.

1.1 1/4 Scale MPD Thruster and Gas Feed System

The 1/4-scale MPD thruster used in this experiment was fashioned after the AFAL 1/2-scale MPD thruster[2]. A schematic of the 1/4-scale device is given in Figure 1. The anode was made of copper, having an inner diameter of 2.5cm and an outer diameter of 4.5cm, while the cathode was made of 2% thoriated tungsten, having an outer diameter of 0.5 cm. The length of the

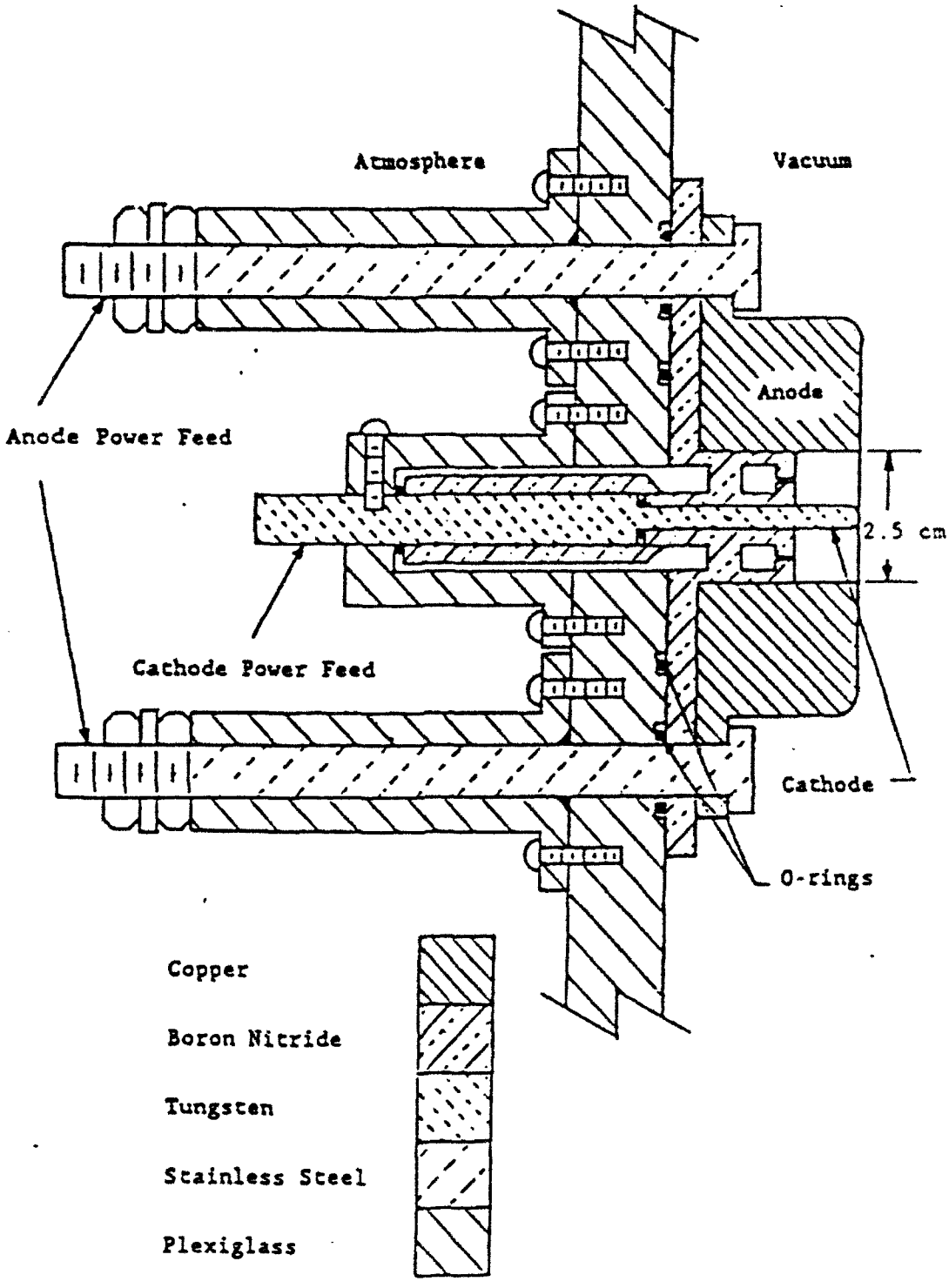

Figure 1: 1/4-Scale MPD Thruster

anode and cathode measured from the boron nitride back plate was 1.25cm. Boron nitride was used to electrically insulate the anode and cathode while serving as a back plate for the discharge chamber. Sixteen orifices were drilled into the back plate to be used as injection ports for the propellant[3]. The thruster quasi-steady current was generated by a tailored-pulse electrical discharge system. The main components of this electrical system included a Pulse Forming Network, a charging circuit, a switch circuit, and a timing system to control the firing sequence[3]. The thruster's PFN L-C ladder is shown in Figure 2. A gas feed system that provided uniform gas flow in the discharge chamber while minimizing vacuum chamber back pressure was designed and constructed. The major components of this system included a reserve plenum, a thruster plenum, and an electrical valve connecting the two plena[3]. A diagram of this system is given in Figure 3.

1.2 Applied Field Magnetic Nozzle

Two applied field magnetic nozzles were built. Two configurations were built to study the effects of changing the penetration time and shape of the magnetic field. The applied magnetic fields were generated by solenoidal coils. The primary nozzle (1) generated magnetic field strengths and shapes similar to those generated by the previous (400 μs) magnetic nozzle[1,2] studies, with the difference being the extended life of the field to improve the magnetic field penetration times. A second nozzle (2), generated the same strength magnetic fields and related penetration times as (1), but the expansion shape of the magnetic field lines was changed. To be able to predict the magnetic field strength and shape a computer algorithm was written. The code allows the calculation of the magnetic field strength using the Biot Savart law[4]. The

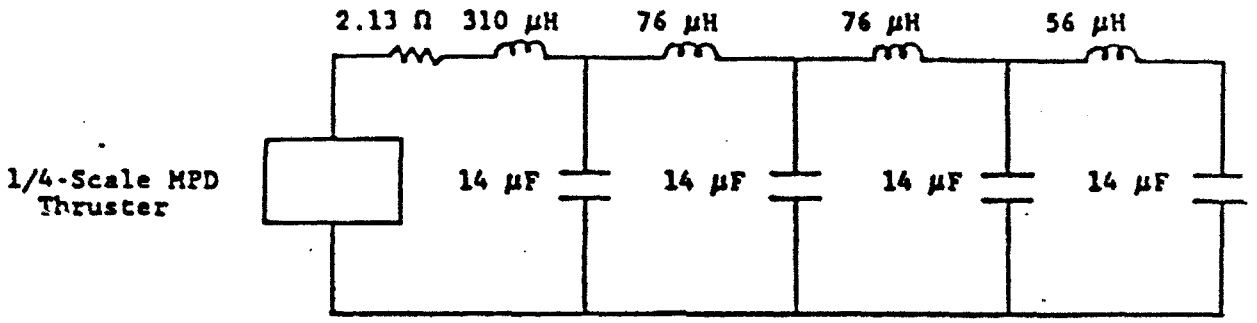

Figure 2: Pulse Forming Networks of Applied Magnetic Field Coil and 1/4-Scale MPD Thruster

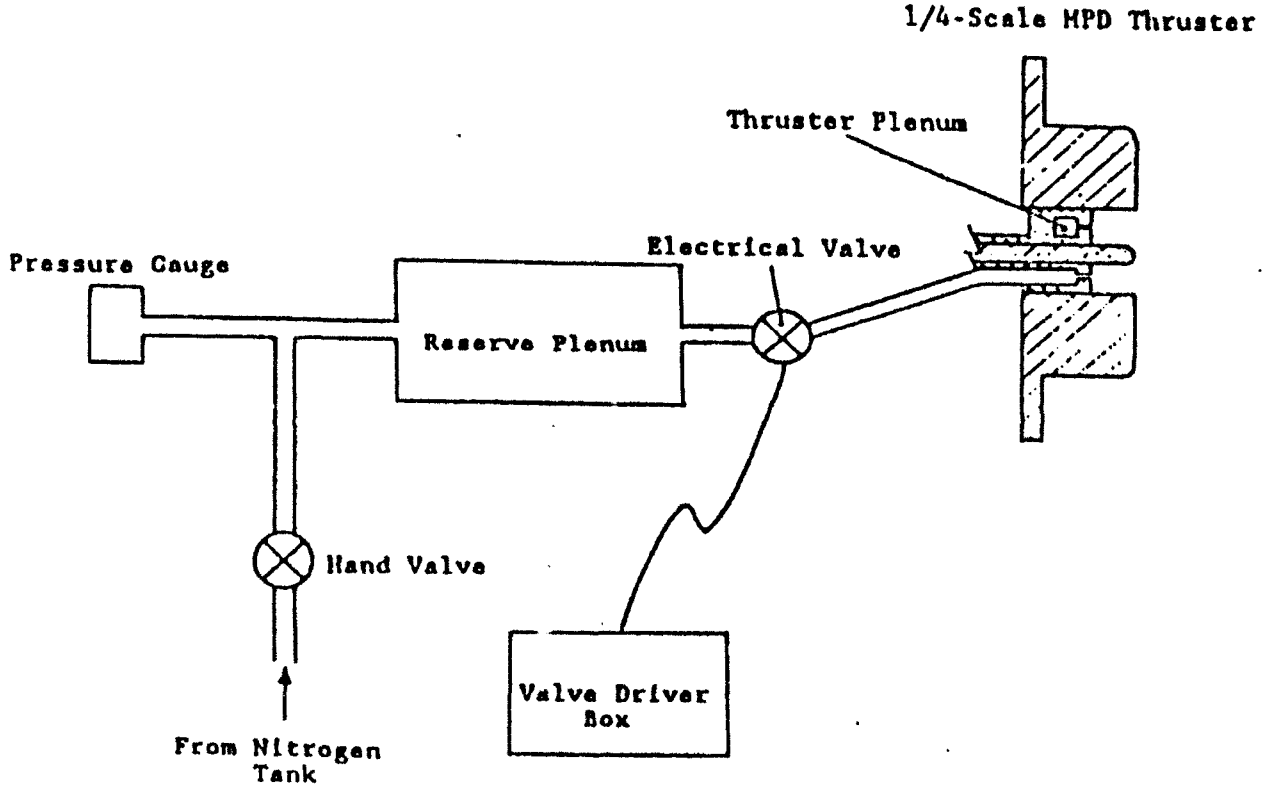

Figure 3: 1/4-Scale MPD Gas Feed System

parameters input to the code include nozzle diameter, arrangement of wire wrapping (number of turns and layers), diameter of electrical wire used in wrapping, and the electrical current through nozzle solenoid. Predicted magnetic field contours for the two nozzles are shown in Figures 4a and 4b.

Nozzle (1) was constructed with 5 layers of 11 wraps of 10 gauge stranded copper wire around an 8.75 in diameter PVC pipe. Nozzle (2) solenoid was constructed with 3 parts: the first part was 7 layers of 4 wraps, the second part was one layer of 1[illegible] wraps, and the third part was again 7 layers of 4; all three parts were wrapped around an 8.75 diameter PVC pipe and they were separated by 3 mm spacers which held the nozzle wraps in place.

With nozzle (1), a current of 500 A generated a magnetic field strength of 1.46 kG at the center of the coil when the face of the thruster was positioned 2.295 cm from the center of the coil.

1.3 Development of High Current Switch for Magnetic Nozzle Current

The current needed to generate fields on the magnetic nozzles coils was supplied by 10, 12 Volt, high capacity batteries connected in series. To be able to accurately control the duration which the large currents (up to 500 Amps) flow through the magnetic coil, a unique switch had to be designed, fabricated, and tested. The design and construction of the magnetic nozzle switch was done by the Electro-Science Laboratory (ESL) at the Ohio State University. Figure 5 presents a schematic of the circuit design. Current flows in the circuit when SCR #1 (Silicon Controlled Rectifier, SK 6787, RCA) is triggered "on". To open the circuit, SCR #2 is triggered "on" thus allowing the capacitors' (GE Motor Run Capacitors, 55 MFD, 550 VAC)

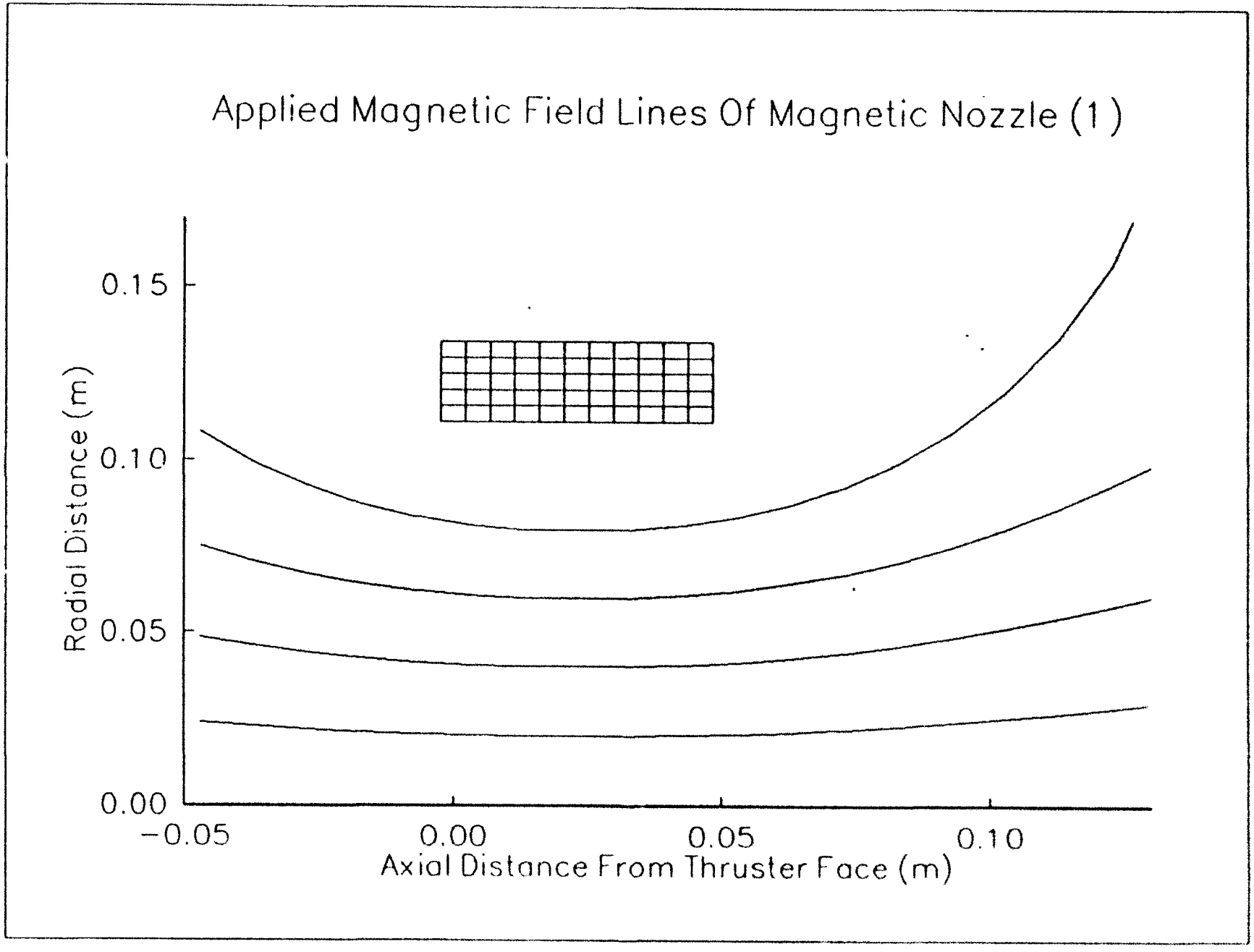

Figure 4a: Magnetic Nozzle Field Line Contours

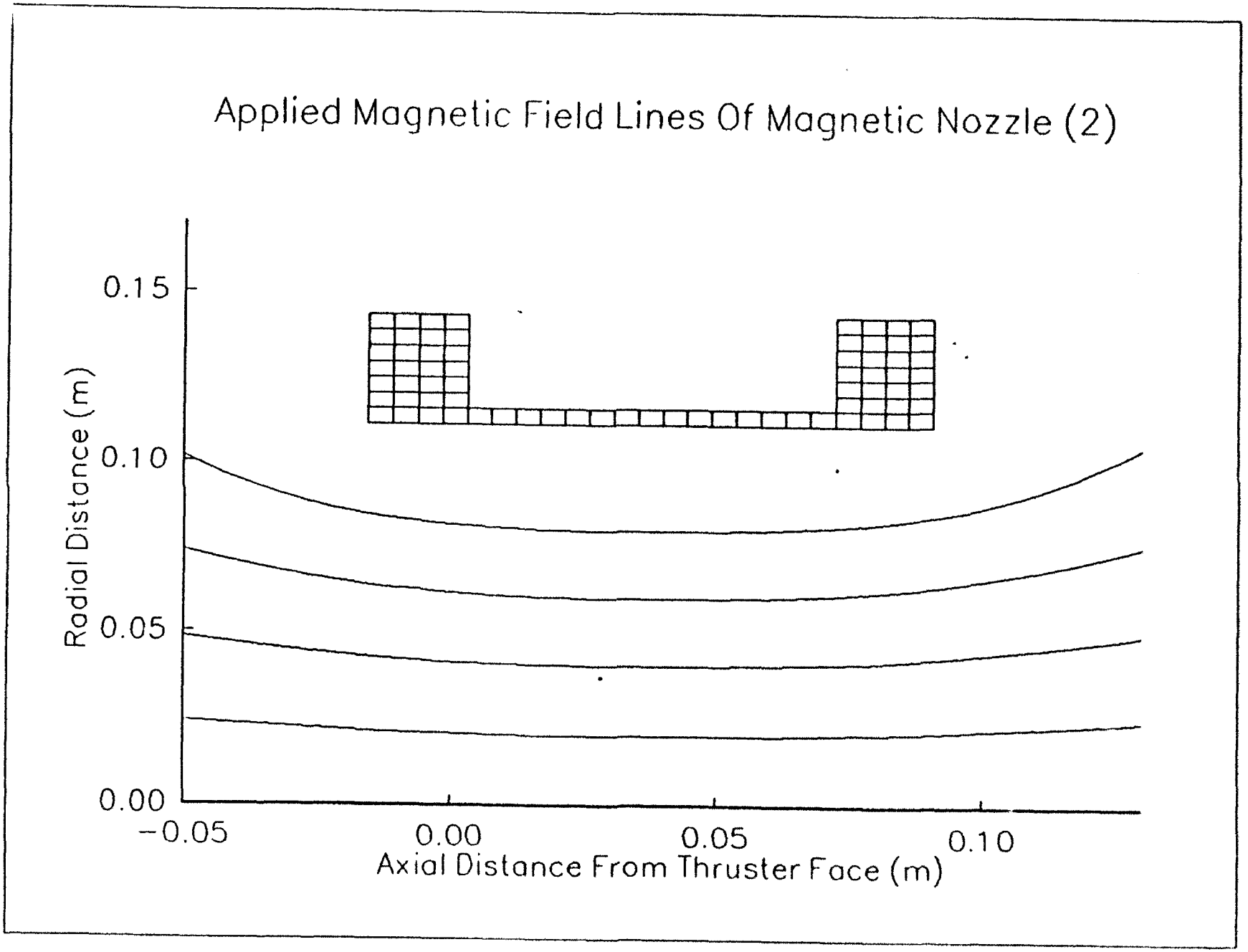

Figure 4b: Magnetic Nozzle Field Line Contours

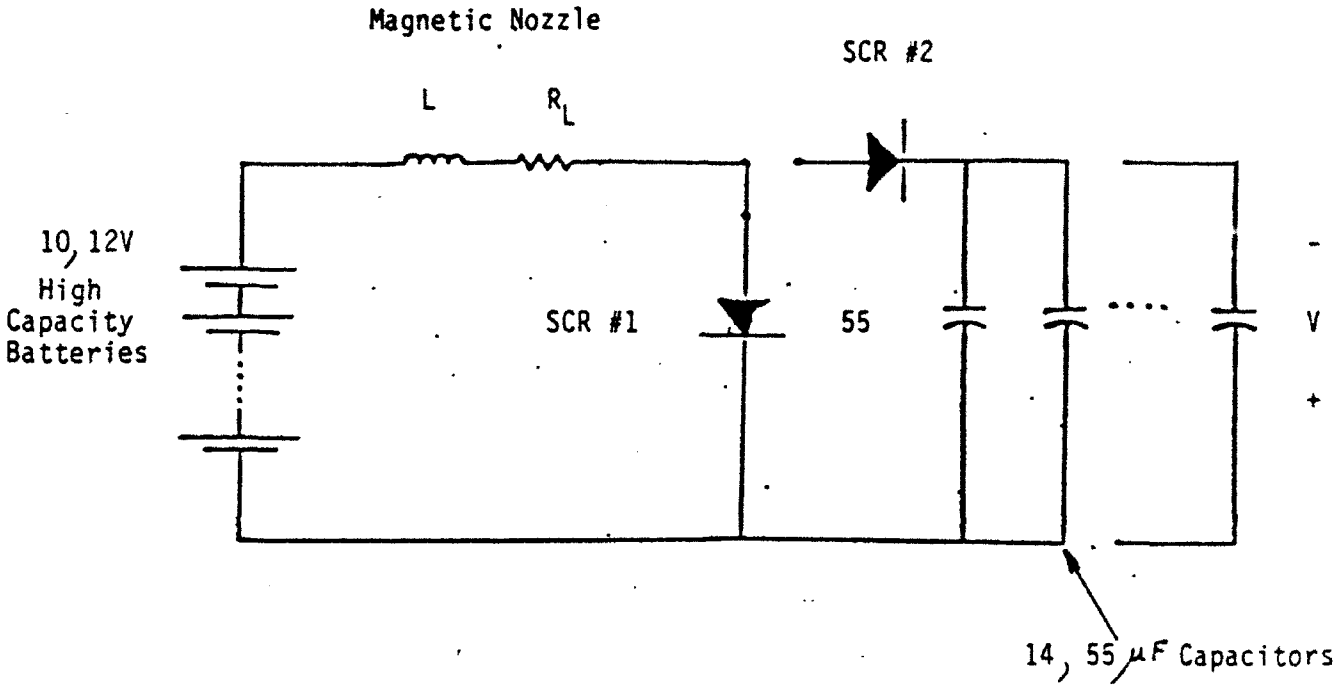

Figure 5: Schematic of Magnetic Nozzle Circuit

negative voltage to switch SCR #1 "off" which in turn opens the circuit. The triggering circuit is outlined in Figure 6.

To be able to accurately set the time duration that the current flows in the circuit, a digital delay generator (Model 7010, BNC) was used as a trigger for the circuit; this allowed penetration times accurate to within 1 msec. The firing sequence caused the circuit to trigger and turnoff appropriately. The batteries and the triggering circuit were placed inside a Faraday cage to eliminate noise triggering and pick up. The trigger signal from the delay generator had to be isolated by the use of an optical-isolator, shown in Figure 7. Testing showed that the triggering circuit triggered correctly for the 1/4-scale MPD thruster operating at or below 10KV. Consequently, it was decided to operate the thruster at current levels at or below 1.675kA.

1.4 Diagnostic Data from The 1/4 Scale MPD Applied Field Thruster

This section presents the experimental data measured for the 1/4-scale thruster utilizing nozzle (1) for different magnetic field penetration times. These ranged from 0 msec (self field) to 500 msec limit. The measurements included: inter-electrode current-voltage characteristics of the thruster, applied magnetic field mapping, impact pressure profiles, electron temperature profiles from Langmuir probes.

The data acquisition procedure was basically the same for all diagnostics. Except for the current and voltage probes the diagnostic device was positioned at the desired location in the exhaust flow . The vacuum pump lowered the pressure in the system to less than 5mTorr. The pressure of the reserve plenum was maintained between 295 and 300 Torr before firing. The capacitor bank of the 1/4-scale thruster was charged to the desired voltage (i.e, 7KV for 1.15kA

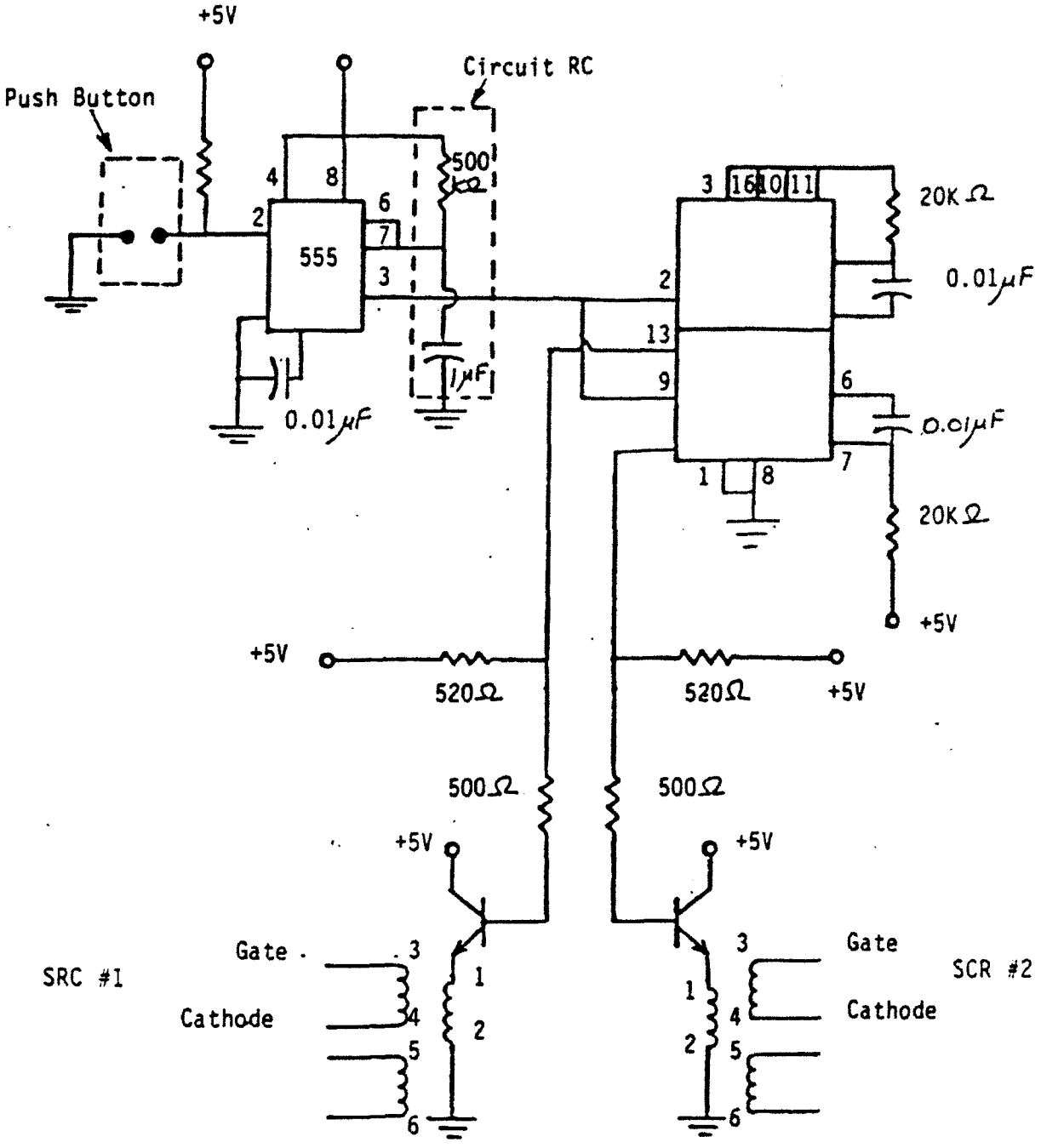

Figure 6: Long Duration, High Current Triggering Circuit

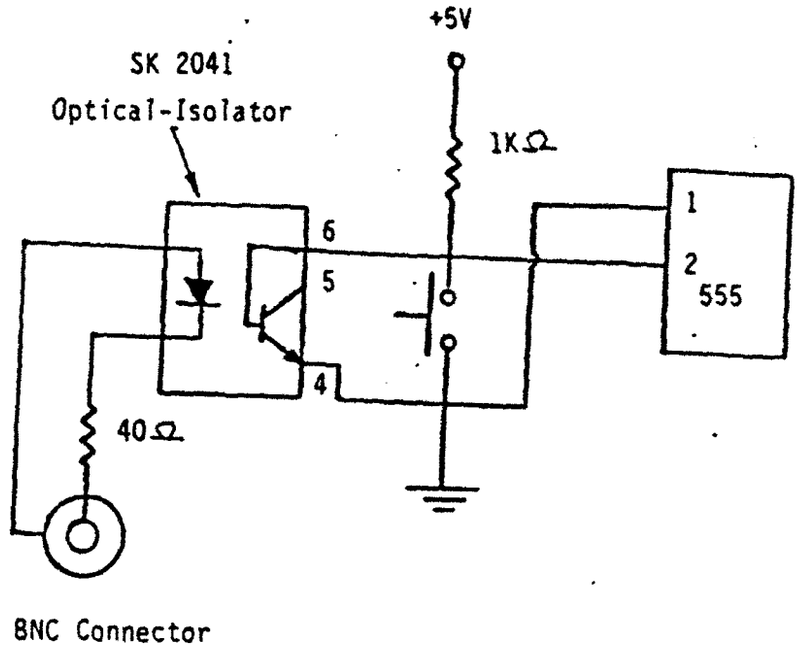

Figure 7: Connection Between Optisolator, Delay Generator, and Triggering Circuit

case, and 10KV for the 1.675kA case). The triggering circuit for the applied magnetic field coil was set for the proper magnetic field penetration time (i.e., 20, 50, 200, or 500 msec).

1.4.1 Current Voltage Characteristics

The current and voltage characteristics for the 1/4-scale MPD thruster with different penetration times were determined with the Rogowski current loop and Tektronix voltage probes[1,2,3]. Typical current and voltage signals are shown in Figure 8a, and 8b. The current and voltages were measured at 200 μsec into the signal. Figure 9 shows the current and voltage characteristics for the various magnetic field penetration times. As reported earlier[1], the thruster voltage for short (400 μs) magnetic field penetration time showed no difference between the self field and applied field cases. Results presented in Figure 9 for larger penetration times contradict the results for short times. It can be concluded that as the magnetic field penetration time increased, the thruster voltage increased for a specified operating thruster current; this is mainly due to the magnetic field penetrating into the inter-electrode region. Thus, earlier results[1] were for an arc-discharge without crossed electric and magnetic fields, whereas present results are for an arc-discharge with crossed field discharges.

1.4.2 Applied Magnetic Field Lines Contours

The magnetic flux lines of the applied magnetic field nozzles were mapped with Hall generator probes. The Hall generator is a four-terminal solid state device capable of producing an output voltage , v_H, proportional to the product of the input current , I_c, the magnetic flux density, B, and the sine of the angle between B and the plane of the Hall generator[5].

Thruster Voltage
20V/div

Thruster Current
965 AMPS/div

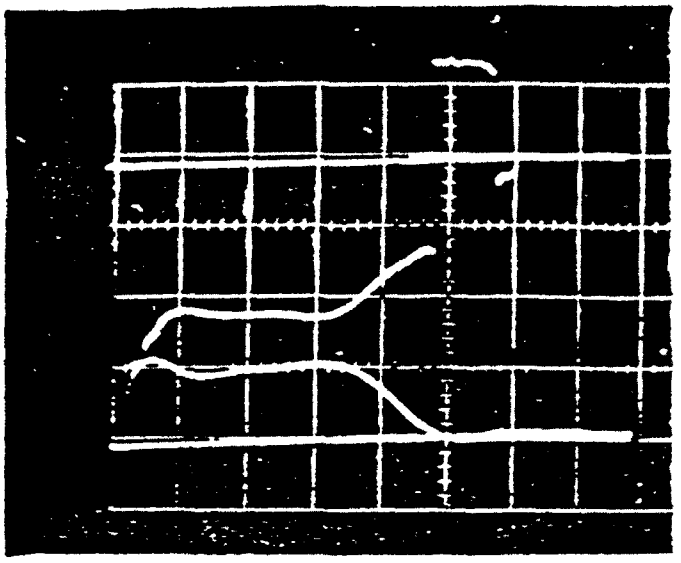

(a)

Thruster Voltage
20V/div

Thruster Current
965 AMP/div

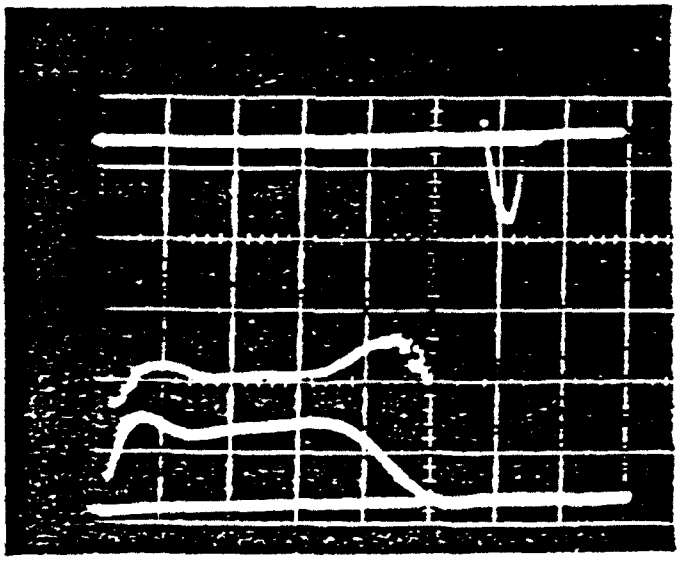

(b)

Figure 8: Typical Current-Voltage Signals

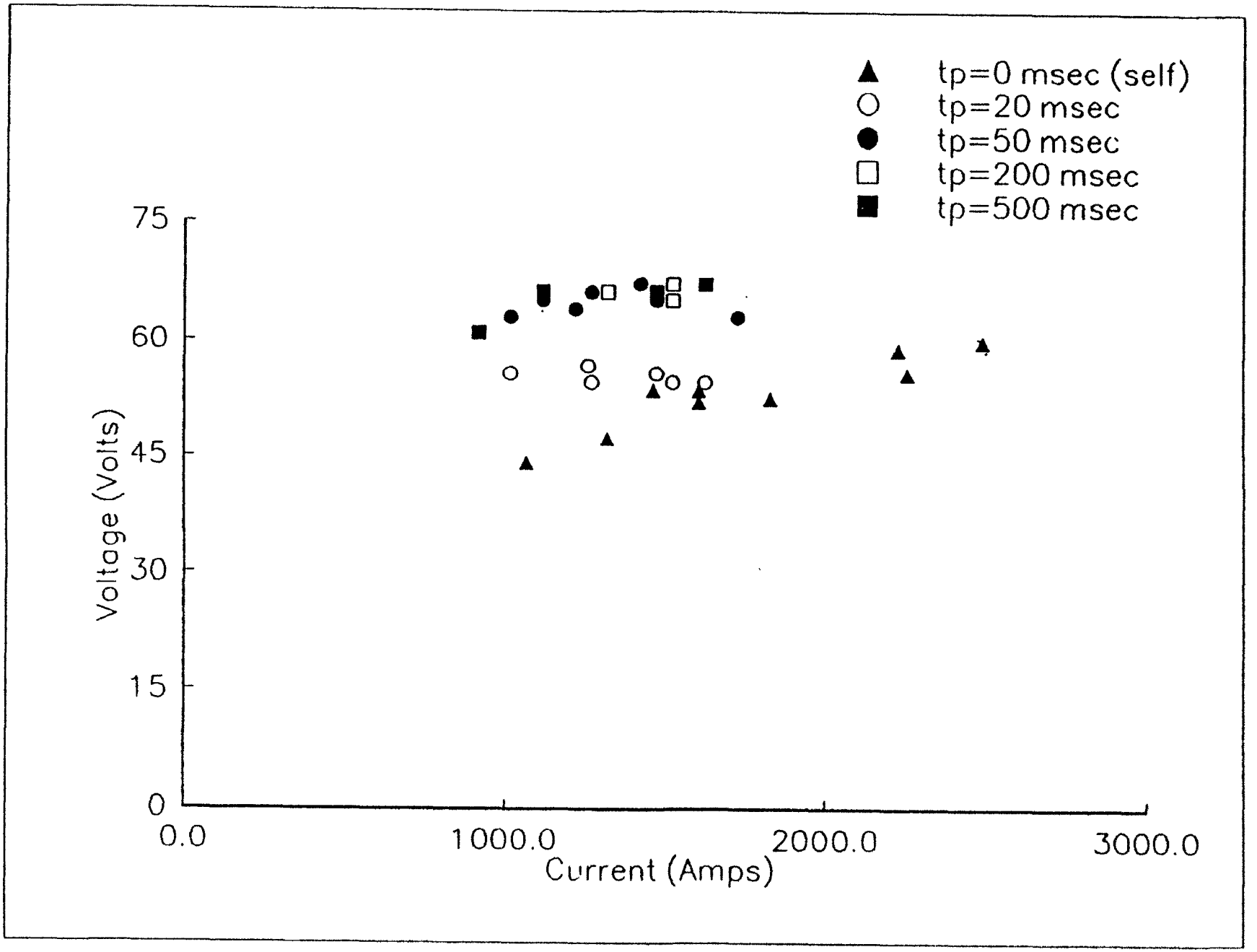

Figure 9: Anode to Cathode Voltage Drop as a Function of Arc Current

$$V_H = \gamma I_C B$$

where γ is the magnetic sensitivity at a specified control current and is obtained from calibration.

Both the axial field Hall probe (Model No. BH-203, 0.06inX0.150in Hall plate, F.W. Bell, Orlando, FL) and the radial Hall probe (Model No. FH-301-040, 0.04inX0.08in Hall plate, F.W. Bell, Orlando, FL) were placed inside the proper size pyrex tubes with fused ends to house the probe head. Coaxial cable (Type 9234, Belden Corp., Geneva, ILLinois) and 28 gauge wire (Type 8066 and 8054, Belden Corp., Geneva, ILLinois) were connected to the Hall probe and ran through the 6 mm pyrex tubing to the probe amplifier and current supply circuit. The Hall probe amplifier was a standard design differential amplifier with a gain of 100 and is shown in Figure 10. The constant control current of 100mA for the axial probe was supplied by the constant current supply circuit shown in Figure 11a. The constant control current of 15mA for the radial Hall probe was supplied by the constant current supply circuit shown in Figure 11b.

The axial and radial Hall probes were calibrated by using a 8.75in outer diameter, 4in long, 15 turn solenoid. In addition, a Helmholz coil was also used in the calibration. The magnetic sensitivity for the axial Hall probe was found to be 6.75 mV/(mA.kG), while the radial/azimuthal Hall probe had a magnetic sensitivity of 135 mV/(mA.KG).

Typical magnetic field signals are shown in Figure 12. The magnetic field strength of the applied field solenoids in the axial and radial directions were determined at axial locations of 1, 3, 5, 9, and 14 cm from the face of the thruster and at radial locations of 0, 2, 4, and 6 cm from the axis. These values are presented in Table (1). At axial locations of1 and 3 cm the

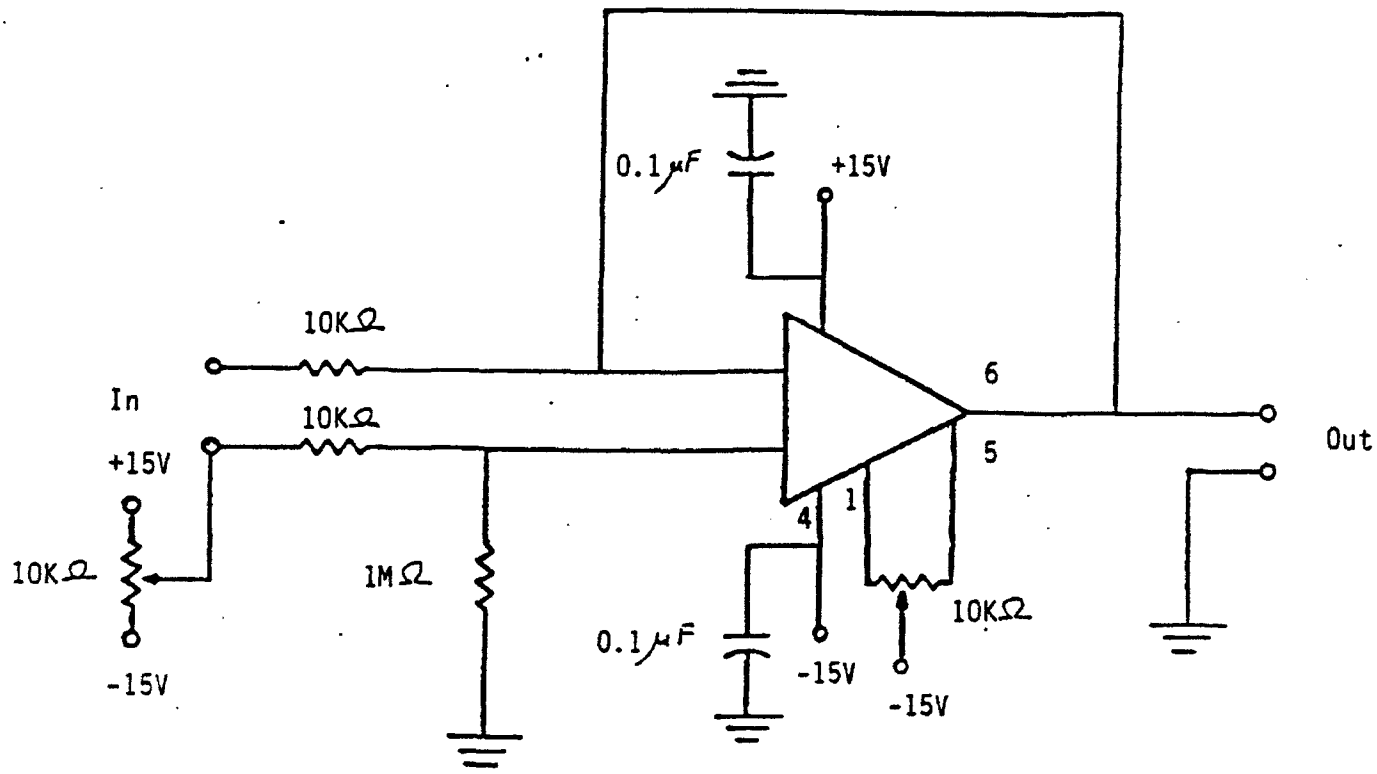

Figure 10: Differential Amplifier

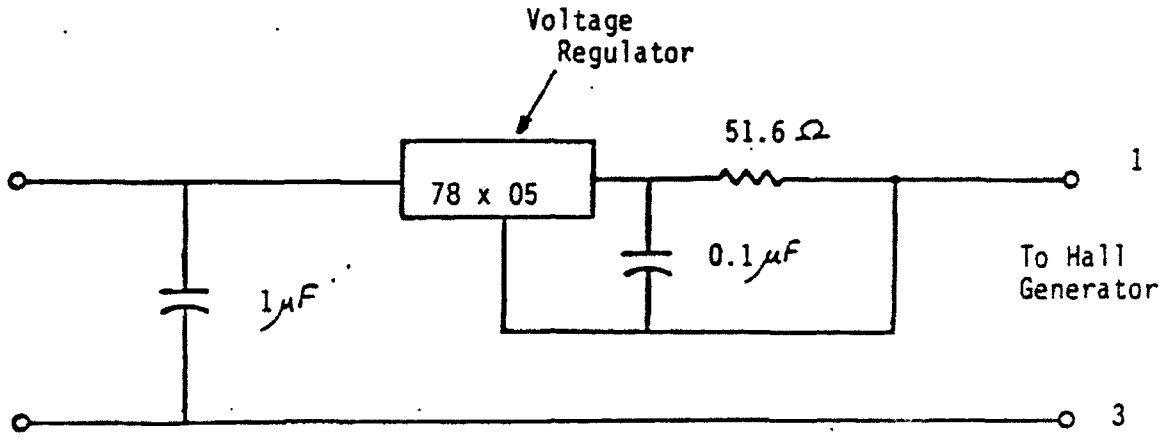

Figure 11a: Constant Current Supply Circuit for Axial Hall Probe

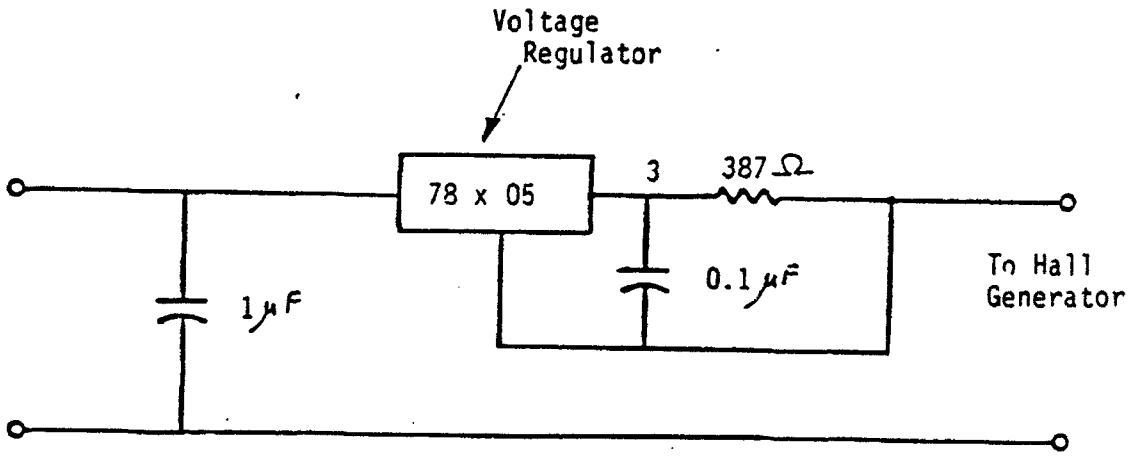

Figure 11b: Constant Current Supply Circuit for Radial Hall Probe

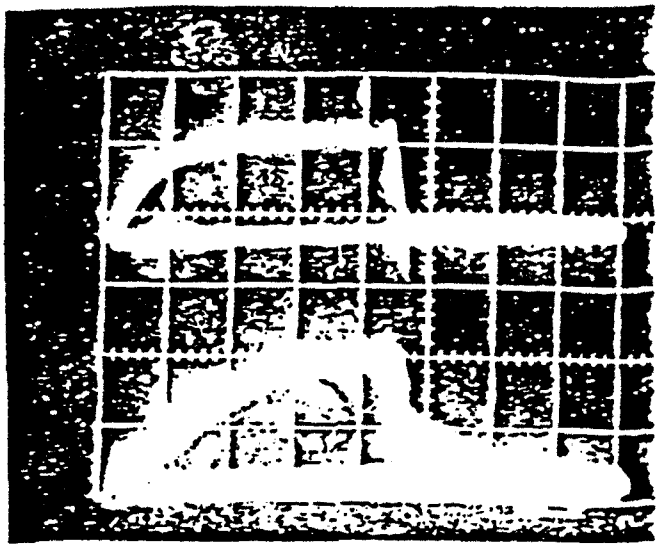

Figure 12: Typical Hall Probe Signals

field signal from the Hall probe lagged the current signal of the magnetic nozzle, as shown in Figure 12; this is due to the time needed to penetrate the inter-electrode region of the thruster. The time for magnetic field penetration is estimated to be 10 msec.

Table (1): Local Applied Magnetic Field Strength Values For Nozzle Number One.

Axial Position (cm) →	1.0		3.0		5.0	
Radial Position (cm) ↓	B (G) Axial	Radial	B (G) Axial	Radial	B(G) Axial	Radial
0.0	1325.5	----	1442.0	----	1364.6	----
2.0	1520.5	----	1637.4	----	1481.5	162.4
4.0	1559.4	----	1715.4	----	1419.1	245.5
6.0	1887.0	----	1949.3	----	1731.0	474.26

Axial Position (cm) →	9.0		14.0	
Radial Position (cm) ↓	B (G) Axial	Radial	B (G) Axial	Radial
0.0	947.7	----	545.8	----
2.0	1013.7	105.7	545.8	75.4
4.0	1029.2	232.7	467.8	117.7
6.0	1052.6	401.7	491.2	184.4

1.4.3 Impact Pressure Profiles

The impact pressure probe that was used was designed and constructed by York[1,2,3]. The output of the probe was matched with an amplifier (X10) and follower circuit and the probe was calibrated by measuring the pressure behind a reflected shockwave in a shock tube; a calibration constant of 3.45 v/psi was obtained[1,2,3]. The radial impact pressure profiles at different axial

locations for the 1/4-scale MPD thruster operating at current levels of 1.15 kA and 1.675 kA with different magnetic field penetration times were determined. Typical pressure signals are shown in Figure 13.

For the thruster operating at 1.15 kA, impact pressure measurements were taken at axial locations of 5, 9, and 14 cm from the face of the thruster and at radial locations of 0, 1, 2, and 3 cm from the axis for different magnetic field penetration times (i.e., 0, 20, 50, 200, and 500 msec). Results are shown in Figure 14.

For the case of the thruster operating at 1.675 kA, impact pressure measurements were taken at axial locations of 5, 9, and 14 cm from the face of the thruster and at radial locations of 0, 2, and 3 cm for the different magnetic field penetration times; results are shown in Figure 15. For Figures 14 and 15, it can be seen that, on axis, the impact pressure magnitude for the applied case (t_p=200 msec) is about 3X the value for the self field case. This indicates that the applied magnetic field is departing more energy in the gas, pinching the plasma, and guiding the expansion direction, whereas in the self field case, the plasma was ejected from the thruster and expanded in all directions.

1.4.4 Electron Temperatures and Number Densities

Electron temperatures and electron number densities were determined in the expanding plasma flow using a double Langmuir probe. A fortunate property of thruster plasmas is that under a wide range of conditions the disturbance caused by the presence of a probe is localized, but in the presence of magnetic fields, the probe interaction is complicated. The principal effect of a magnetic field is to confine electrons and ions within

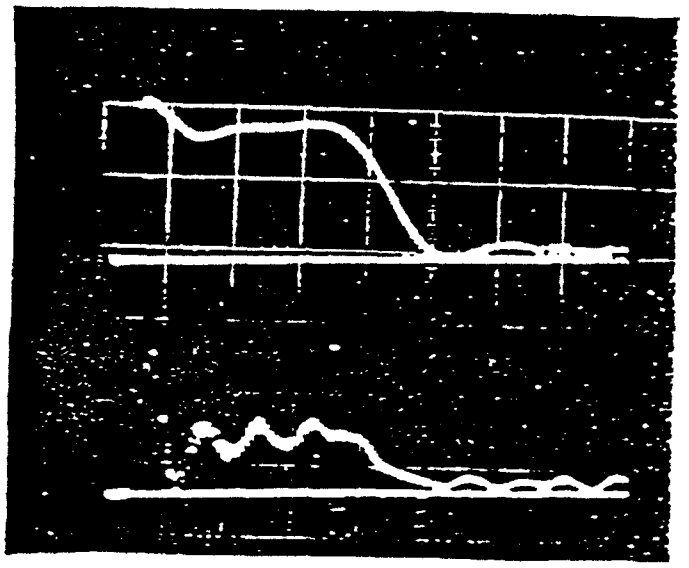

Figure 13: Typical Impact Pressure Probe Signals

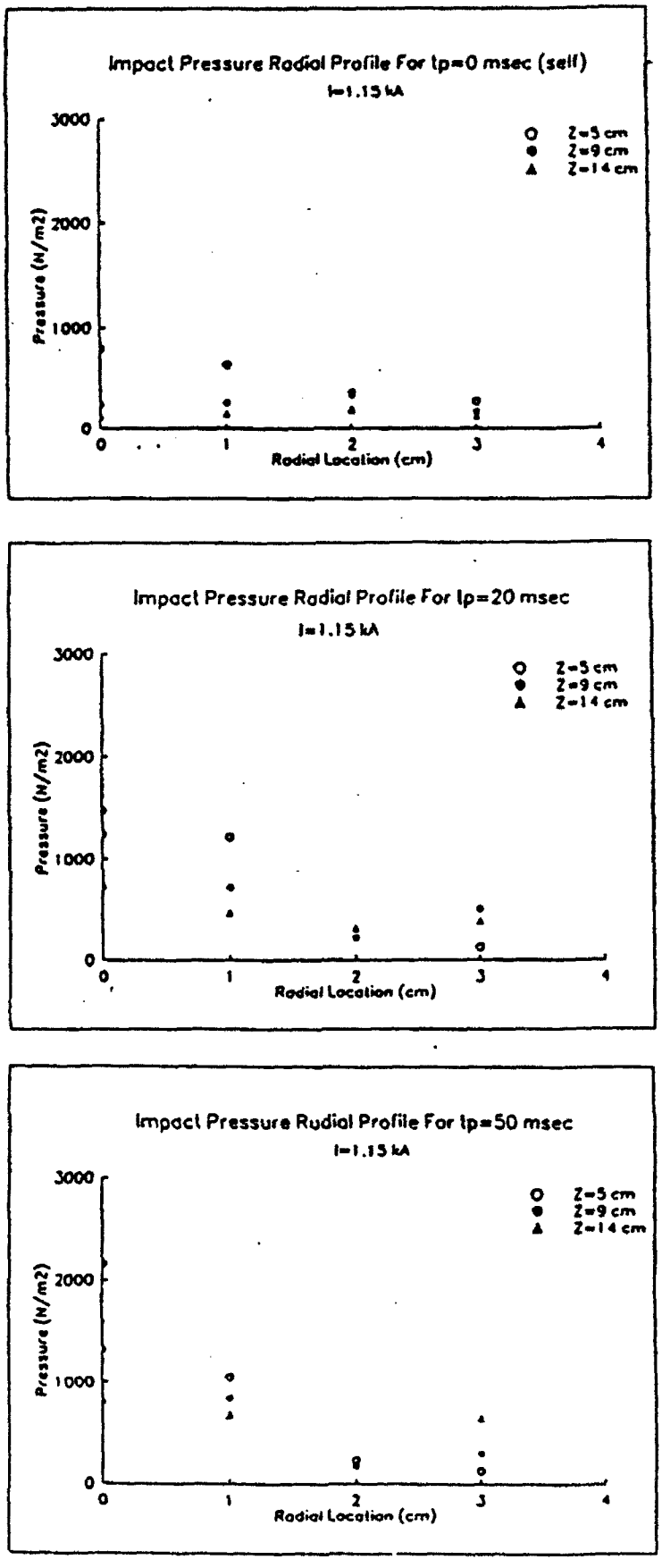

Figure 14a: Impact Pressure Measurements with I = 1.15 kA

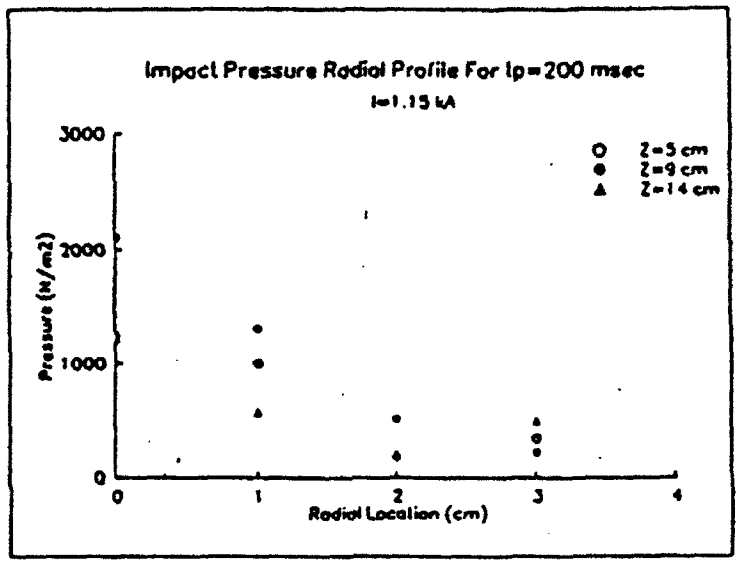

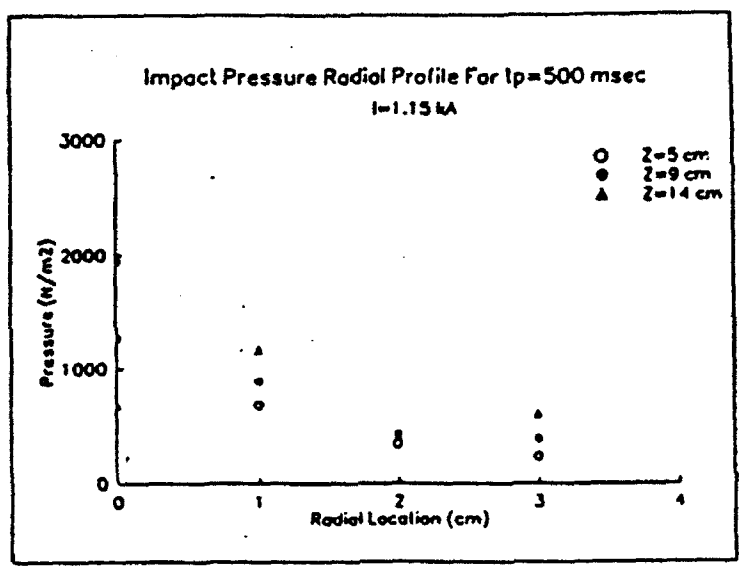

Figure 14b: Impact Pressure Measurements with I = 1.15 kA

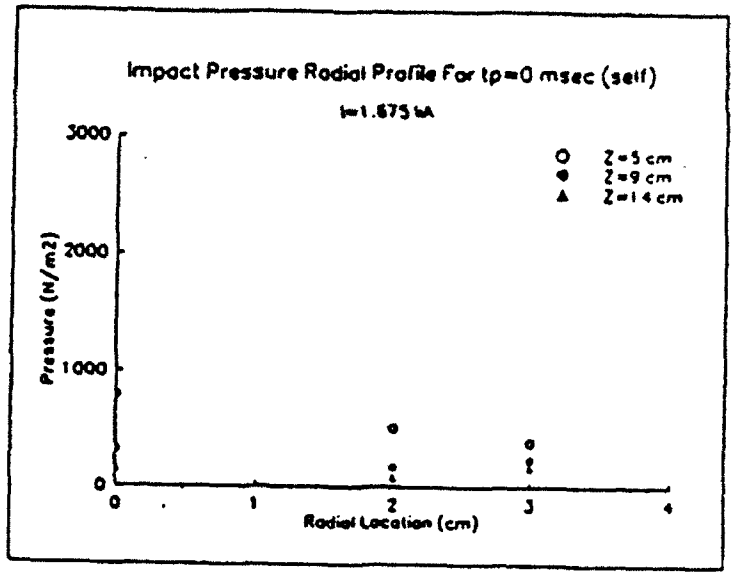

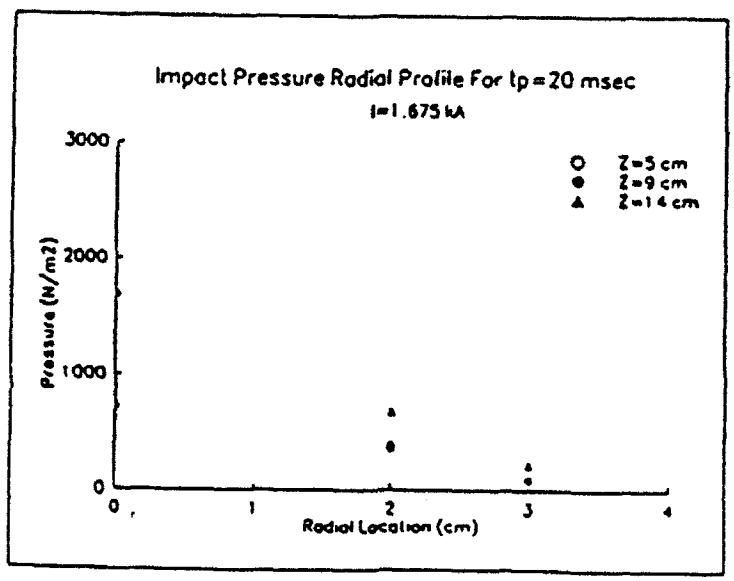

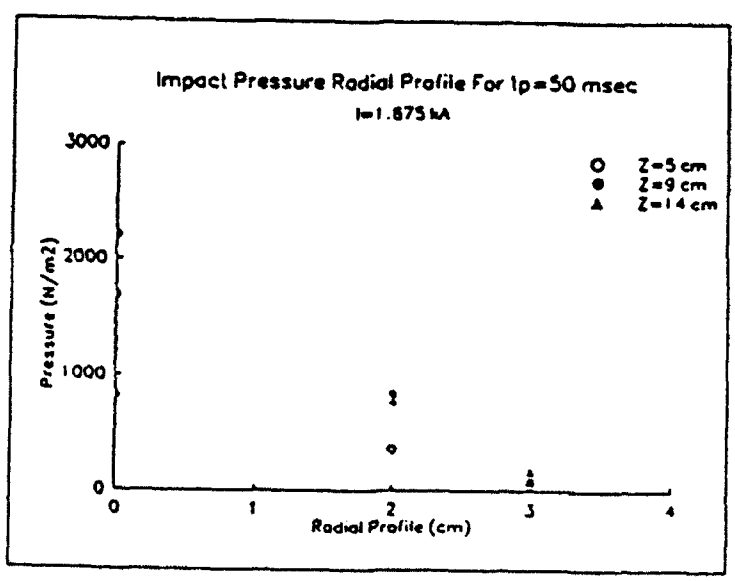

Figure 15a: Impact Pressure Measurements with I = 1.675 kA

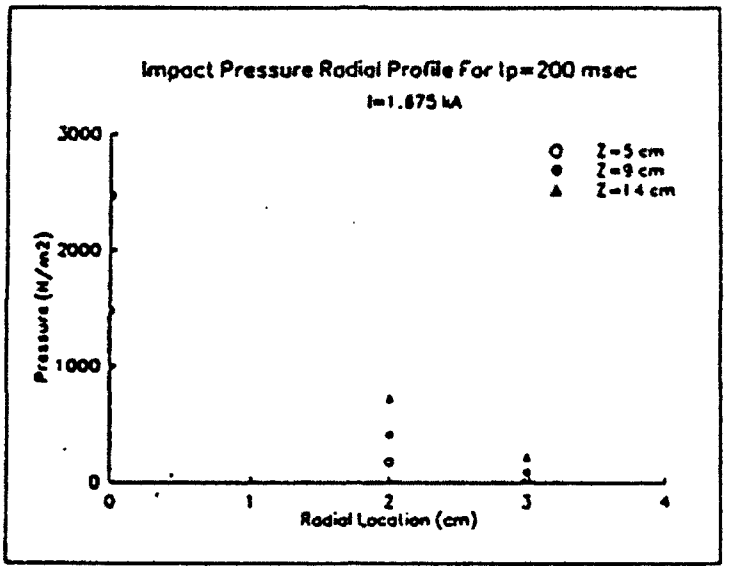

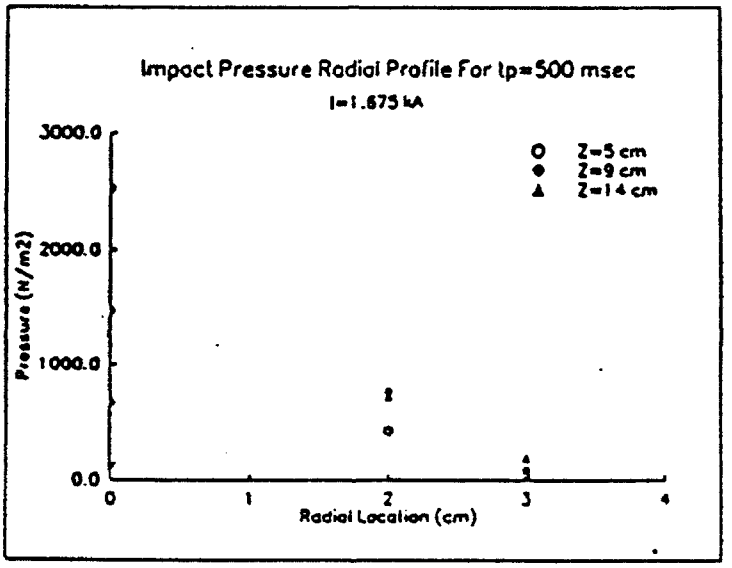

Figure 15b: Impact Pressure Measurements with I = 1.675 kA

a Larmor radius and consequently depress the diffusion of electrons and ions across the field[6]. It is of great importance that before the effects of magnetic fields are taken into account, a careful determination of the probe regime of operation be made. This determination is made by a evaluation of a number of parameters that relate to the collision mean free path (λ)[7], Debye length (λ_D)[7], probe size (r_p), and Larmor radious ($r_{Li,e}$)[7,8]. A determination of whether magnetic field effects are significant is primarily arrived at by comparing $r_{Li,e}$ to r_p. If $r_{Li,e} >> r_p$ then the analysis of zero magnetic field is applicable[6,8]. Using the T_e and n_e values obtained in earlier work, it was estimated that the analysis for a zero magnetic field is applicable. However, the T_e and n_e values measured in this research effort are significantly different and may redefine the Langmuir probe regime of operation. Thus a better understanding and subsequently a better determination has to be made of the Langmuir probe regime of operation.

For the double Langmuir probe used, the probe elements were made of 0.127 mm diameter tungsten wire, had an exposed length of 10 mm and were separated by a distance of 5 mm[1,3]. The voltage bias across the probe elements was accomplished by a floating prob circuit[3]. In order to avoid distortion of the electrostatic probe response by surface contamination, chemical cleaning was used periodically while glow cleaning was used after each shot[8].

Electron temperatures were determined from a graphical evaluation of the voltage current characteristic curve recorded for the double Langmuir probe. For the self-field($B_{app}=0$) case ($t_p=0$ msec), data were taken at axial locations of 5, 9, 14, and 20 cm for the 1/4-scale MPD thruster operating at 1.15 kA, and 1.675 kA, respectively. For the applied field cases, data

were taken at axial locations of 9, 14, and 20 cm; results could not be obtained at Z=5 cm since data taken at that point were distorted apparently because of the probe element proximity to the thruster electrodes. Table 2 presents electron temperatures at various axial locations for the self and applied field cases.

Table (2): Electron Temperatures For The Self and Applied Field Cases at Z=9, 14, and 20 cm.

Axial Position (cm)	Self Field T_e		Applied Field T_e	
	1.15 kA	1.675 kA	1.15 kA	1.675 kA
9	0.580	0.683		
14	0.506	0.893	3.578	
20	0.502	0.969	1.506	1.6362

In addition, for the applied case data were only taken at t_p=200 msec mainly because the impact pressure data indicated that at that magnetic field penetration time, effects of the applied field were fully realized. Figure 16 shows a typical Current-Voltage characteristic curve of a double Langmuir probe at Z= 20 cm for both the self and applied field cases at a thruster current of 1.675 kA.

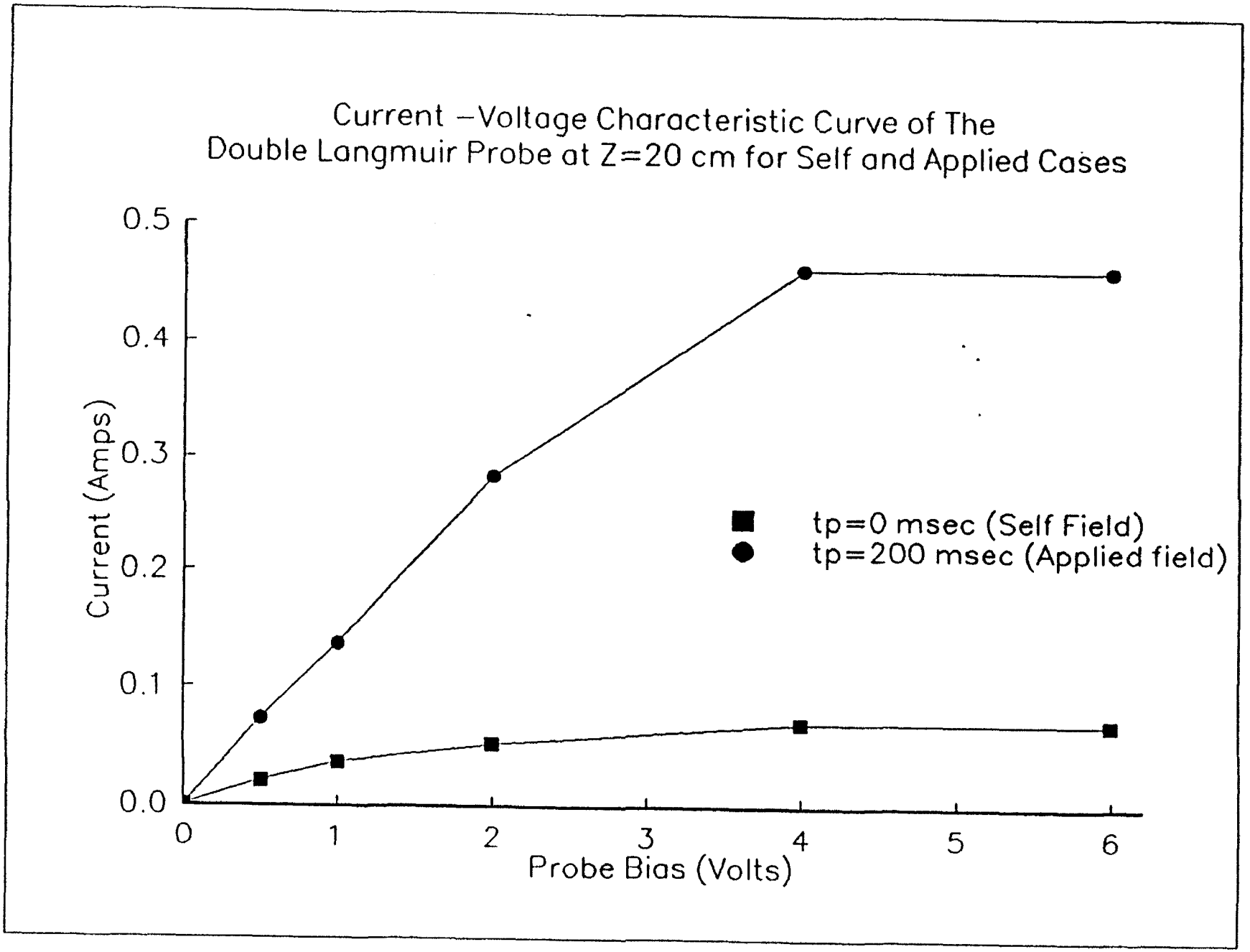

Figure 16: Typical Double Langmuir Probe I-V Characteristic

2. Multi-Beam CO_2 Interferometer Study of 1/4-Scale MPD Plasma
(Ke-I Li)

During the past two decades, many reported works have been dedicated to the study of the operational capabilities of MPD thrusters. Only recently has the research emphasis shifted toward the investigation of erosion instability and lifetime reliability of thrusters. Yet, to date, little progress has been made on the identification of mechanisms of heating and acceleration in the MPD thruster, due primarily to the inadequacy of the diagnostic techniques applied. There is only one way to reach an improved state of understanding of MPD operational capability, and that is the utilization of non-intrusive diagnostic techniques to provide new, local data on the acceleration mechanisms.

This study is intended to provide experimental data on arcjet and MPD arc thrusters radial and axial electron density distributions. This research has two objectives. The first is to experimentally examine the dominant acceleration mechanisms in the (selt-field) arc MPD thrusters through Ne studies. The second is to construct the history of density profiles in the applied-field magnetic nozzle of a MPD thruster so that the expansion process can be carefully studied.

2.1 Definition of the Uniqueness of the CO_2 Interferometer

When an electromagnetic wave (laser light) propagates in a plasma it undergoes a phase shift which is given by :

$$\Delta\phi = 2.82 * 10^{-13} \lambda_0 \int_{z_1}^{z_2} N_e(Z)\, dz\, (cgs)$$

where $\Delta\phi$ = the phase shift

λ_0 = the wavelength of the radiation
$N_e(z)$ = the chord dependent electron density

The sensitivity of an optical interferometer is defined in terms of the minimum detectable electron density, ignoring the contributions of the nonelectronic component of the plasma. Consider a fringe shift ($\Delta\phi/2\pi$) relative to vacuum caused by an electron density of of N_e cm^{-3} in a path L. With detection of one hundredth of a fringe, the minimum value of N_e discernible will be :

$$\frac{\Delta\phi}{2\pi}=\frac{1}{100}=2.82x10^{-13}\lambda_0 xLxN_e$$

and with L=10 cm, and $\lambda_0(CO_2)=10.6x10^{-4}cm$, $(N_e)_{min}=10^{12}cm^{-3}$. Such a diagnostic was successfully applied to a ZT-40 Machine at Los Alamos National Laboratory by A.R. Jacobson[9]. With its long wavelength 10.6μm, the CO_2 laser interferometer was able to generate spatial resolution of the plasma inside the ZT-40 machine with a sensitivity up to one thousandth of a fringe shift (Fig.17).

The plasma ejected from MPD type devices has been categorized by a number of research studies. At Ohio State University, Langmuir probe study on a 1/4-scale MPD thruster was reported and indicated that the number density varied from 10^{15} to 10^{13} cm^{-3} and Te = 0.5-1.5 eV at 5-20 cm. The CO_2 laser interferometer development was pursued here because with a sensitivity of $(N_e)_{min}=10^{13}cm^{-3}$, it is capable of detecting the electron density inside a 1/4-scale MPD thruster exhaust flow.

In order to establish the capablity of the CO_2 system, a brief review of other possible interferometer systems will be presented. A Fabry-Perot interferometer system (FPI) has a more complicated configuration than the CO_2 interferometer. The sensitivity of a FPI to plasma line

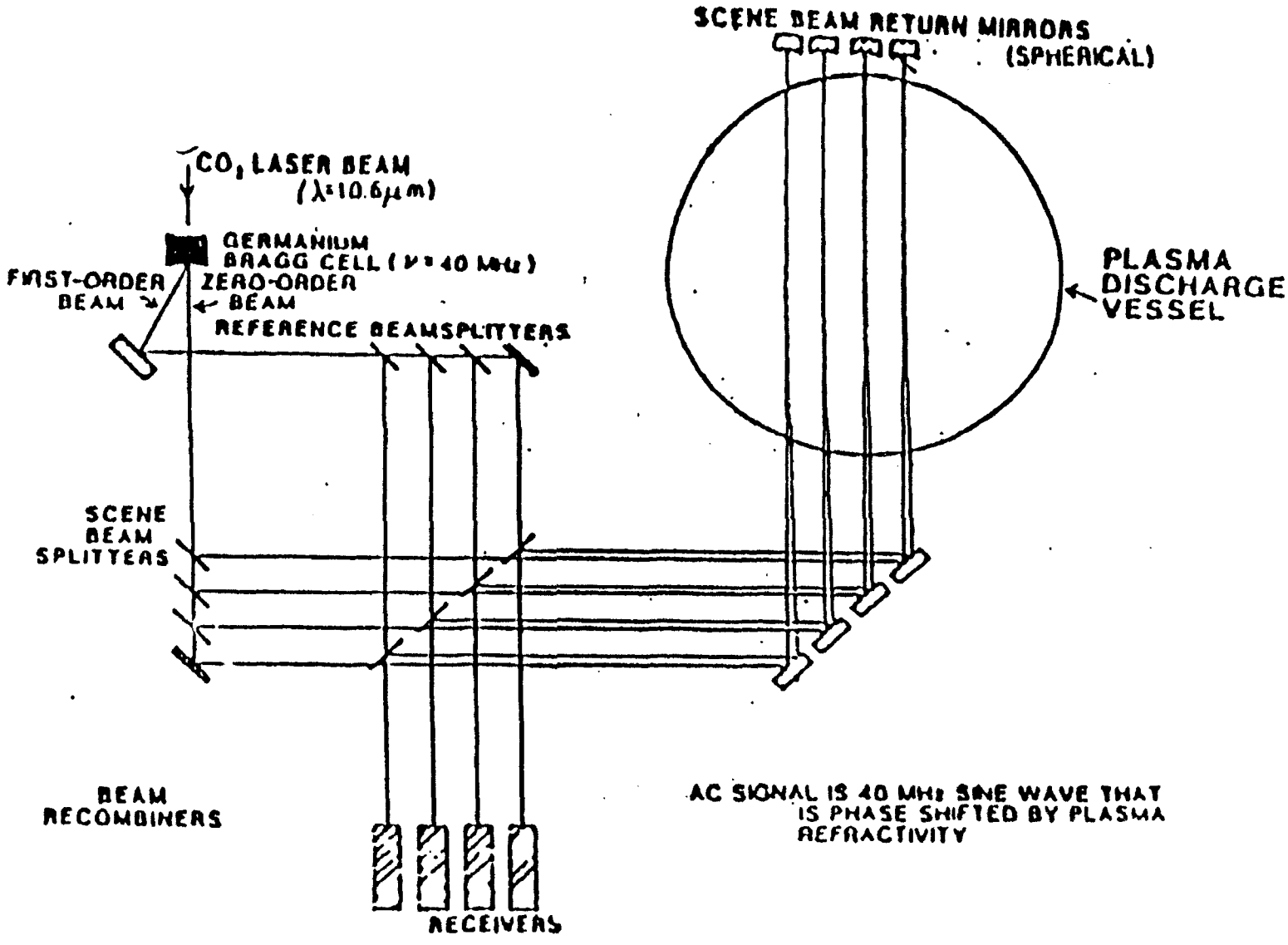

Figure Schematic of Multi-Beam Interferometer

densities is not only proportional to the wavelength but also the finesse of the optics whereas the sensitivity of the CO_2 interferometer is fixed only by the wavelength of the CO_2 radiation. The FPI system can be made more sensitive than other interferometer only at very specific mirror positions. Thus, for the FPI to function properly, the mirrors must be at precise distances from one another.[10] This tends to make the alignment of the FPI system very critical to achieve a high sensitivity. Another limition results from the cavity size. Therefore, the FPI device is limited in its sensitivity to plasma line density within 10^{14}-10^{15} cm^{-2}. Compared to FPI system, the CO_2 interferometer clearly has a higher sensitivity with a minimum detectable plasma line density of $10^{-13}cm^{-2}$.

2.2 Heterodyne Detection Techniques

The CO_2 laser interferometer geometry to be described here utilized heterodyne detection. An acoustic-optic (Bragg) cell (Intra-Action Corp. Model AGM-406b) was used to angularly separate the CO_2 laser beam into two output beams which are also separated in frequency from each other by 40MHz. The acousto-optic cell acts as the initial beamsplitter of the interferometer, and the reference beam frequency shift facilitates heterodyne detection of the electron refractivity. In the CO_2 laser interferometer, the beam that has passed through the plasma (scene beam or zero order beam) is phase modulated by the changing refractive index of the plasma. The scene beam is recombined with the reference beam, and the output contains sum and difference frequency components, that is, if the frequency in the reference arm is ω_1 and that in the scene arm is ω_2, the output contains frequencies $\omega_2+\omega_1$ and $\omega_2-\omega_1$, only the low frequency $\Delta\omega$=40MHz will be of interest here.

If there was no frequency difference between the scene beam and the reference beam, when the scene beam was phase-modulated by the refractive index of the electrons, the frequency difference between two beams is not zero. However, it is generally not possible to distinguish between positive and negative $\Delta\omega$. This is the cause of ambiguity of phase change direction[11].

An acousto-optic cell (Bragg) in the CO_2 interferometer configuration generates a frequency difference between the scene beam and the reference beam. Even when the plasma phase shift is constant, the frequencies of the two beams are no longer equal and the output contains a signal at frequency $\Delta\omega$=40MHz. Therefore, when additional frequency modulation occurs, due to plasma phase changes, the output frequency thus increases or decreases according to the direction of phase change, and ambiguity in direction is not present.

2.3 The CO_2 Laser Interferometer

A schematic of the interferometer system is shown on Fig.18. To date, the interferometer components have been assembled and tested. The system has not yet been operated successfully, primarily due to continuing difficulties with the detector system supplied by Electro Optical System Inc.,Phoenixville,PA. This will be discussed further below. The performance characteristics of the components will be discussed in detail. First the ideal operation of the interferometer will be discussed.

The CO_2 laser system (Apollo Laser Inc., Model 122) consists of a tunable CO_2 laser (Model 570) and a FIR resonator fully integrated. Model 570 which serves as the optical pump for the submillimeter resonator is tunable to more than 85 wavelengths in the 9.17 to 10.91

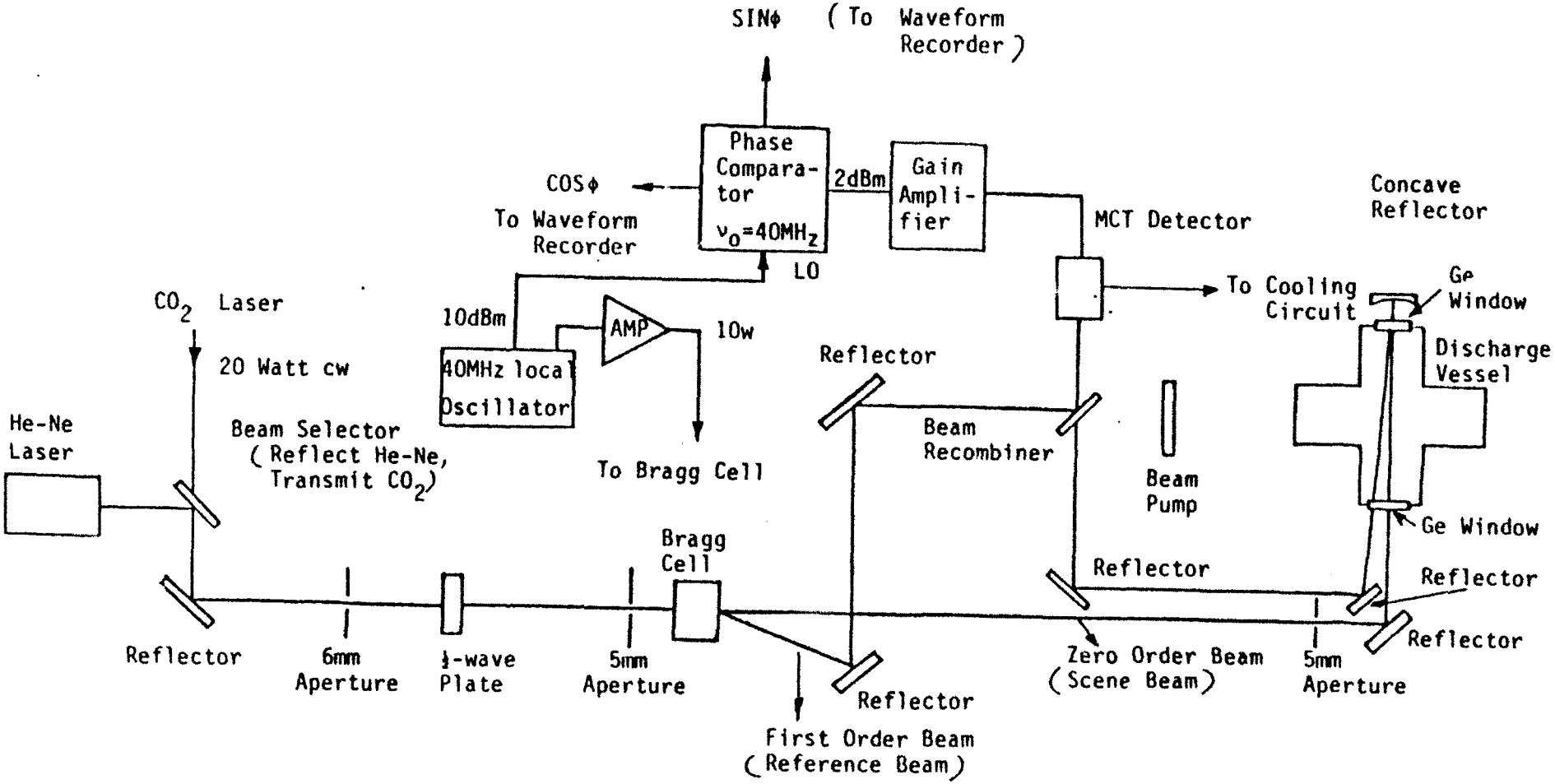

Figure 18: CO_2 Laser Interferometer Schematic

micron range. It can be operated in CW, chopped or pulsed mode. The submillimeter waveguide resonator is a variable length Fabry-Perot resonator. It includes the appropriate hole-coupled reflectors to allow oscillation over a wide range of far infrared wavelengths. The laser system is coupled with a CO_2 laser cooling system (Neslab, Model RTE-110B) Which is a constant temperature bath operating between -30 degrees C and +100 degrees C. The system is equipped with a circulating pump which circulate the water through the CO_2 laser systm. The desired bath temperature is set on the temperature controller and the temperature was kept at 23 degrees C during the experiment.

After assembly and testing it was found that the output power of the laser system in the TEM_{00} mode ranged from a minimum 20 Watts to 55 Watts on the strongest lines. This laser system exhibited output variations at power levels of 40-30 Watts CW (Fig.19). This effect was avoided by operating the laser system at 20 watts CW. The output beam, with a divergence angle of 3 mrad, was down-collimated from an 8mm diameter to a 5mm diameter, and it then entered a half-waveplate (Incorp, Series WPM-10.6) to rotate the polarization of the incident laser beam by 90 degrees and thus make the beam horizontally polarized. This was necessray to achieve a workable interferometer layout. The beam then went into the acousto-optic cell (Intra-Action Corp. Model AGM-406B). The AGM-406B acousto-optic cell utilizes Bragg deflection of light by an acoustic beam. If the incident light beam strikes the acoustic wave fronts at a proper angle, the Bragg angle, efficient deflection of the light beam occurs. At 10.6μm wavelength the Bragg angle was approximately 2.21 degrees. The diffracted beam was also upshifted in frequency by an amount equal to the RF carrier frequency (40MHz). This experiment required the RF signal that drove the acousto-optic cell be synchronous with the

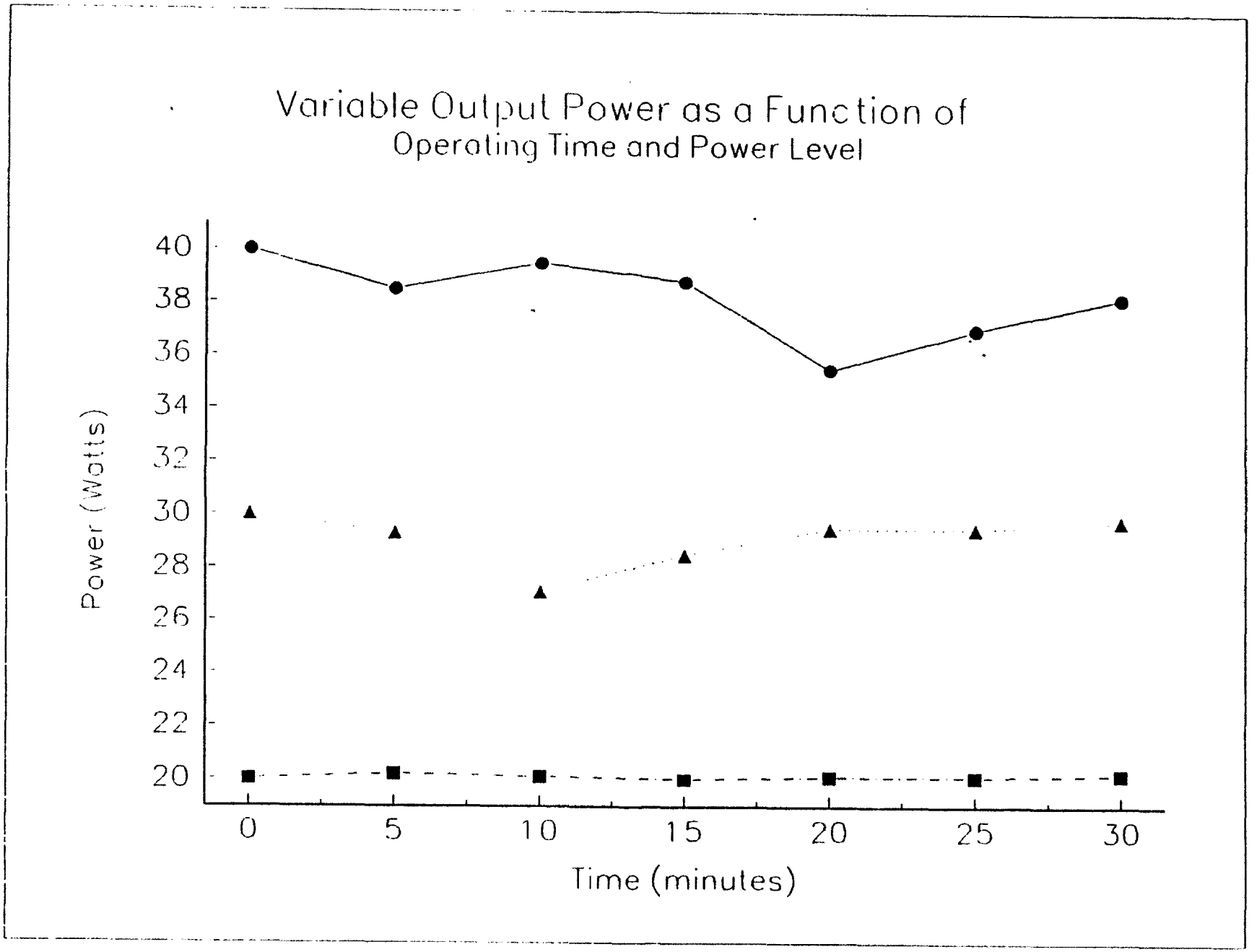

Figure 19: Variation of Output Power over a Period of Time for Different Power Levels

reference signal that drove the quadrature phase detectors. Thus the driver of the cell (AGM-408C) was modified to supply two reference signals (40MHz) each at +10dBm. The acousto-optic cell separated the beam into the scene beam (zero-order) and the reference beam (first-order), whose frequency was shifted up by 40MHz with respect to that of the scene beam. The power level was kept at 100mw in each beam. The scene beam passed to a reflector outside the vacuum chamber and then horizontally through the plasma. The beam was then reflected back through the plasma and onto the beam recombiner. All the partial mirror optical components (Optics for Research,) were made from zinc selenide were AR-coated on the second surface and custom-coated for specified reflectivities on the first surface. A portion of the reference beam returning to the recombiner was sent to its detector (Electro-Optical Systems Inc., Model MCT10-T1-002) along the same path as its reference beam.

The detector is a photoconductive HgCdTe (Mercury Cadium Telluride) device designed specifically to detect CO_2 radiation. The unit includes the detector module, typically with 20 to 50 Ohm resitance, a two stage thermoelectric cooler with a thermistor type temperature sensor, a sealed package/heat sink with germanium window AR coated for 10.6 microns with a CO_2 radiation sensitive area of $4mm^2$, a gain amplifier (Model EM-40) and signal conditioning electronics. When the radiation was detected by the detector, a signal proportional to the input power was generated and amplified.

Testing of the detectors was done at two different beam modulation frequencies. The detectors were first placed before the Bragg cell and operated at -30 degrees C. An optical beam chopper was put into the laser beam with a chopping frequency set at 4kHz. The beam diameter was 5mm and the power level in the beam was kept at less than 200mW onto the

detectors surface. The detector output was amplified and displayed on an oscilloscope. It was found that one (most sensitive) detector (cooled at -30°C) exhibited a responsitivity of 9.1 volts/watt at 4kHz. This result was close to what the manufacture specified: 10 volts/watt at -30°C, but the detectors were also specified to be used with the 40MHz signal.

The detectors were then tested with the 40MHz beam modulation frequency. The whole interferometer circuit and the Bragg cell were operated as described above. A recombined beam power of 200mw with a 5mm diameter was sent to the detector. Due to the Bragg cell, the detected signal contained a 40MHz (Beat Frequency) amplitude-modulated component caused by the interference between the reference and the corresponding scene beams. There was no output signal. The amplified beat frequency signal was found to be only 5mV(pk). This intensity was not enough to drive the quadrature phase comparator (Merrimac Industry Inc., Model PCM-3-40B).

The amplifiers were tested for output performance in the following fashion. A sine wave signal of 10mV(pk) at variable frequencies was output from a function generator (Wavetek, Model 166) with a 50Ω output impedance. The signal was first viewed on the oscilliscope (Tektronix, Model 7603) and then connected to the amplifier with a RG58/U cable plus a 50Ω terminator at amplifier input. The amplifier output signal was connected to and viewed on the scope with a 50Ω terminator coupled at the end of the short RG58/U cable. Generally, the output from the amplifier was about 1volt(pk) at frequencies from 4kHz to 10MHz, (gain of 100 from 4kHz to 10MHz). Gain then dropped to 50 at 20MHz and to 10 at 40MHz. This was unsatisfactory output performance for the experiment being conducted. The amplifiers have been shipped back to the manufacturer for redesigning to achieve higher gain at frequency of 40MHz.

An eight channel waveform recorder (Gould Electronics, Model 4386) was procured to digitize and store the sine and cosine signals from the phase comparators. It is equipped with eight single ended channels each one having its own 8-bit A/D converter. The input measurement range varies from 50mv to 500 volts full scale in 13 calibrated input ranges with variable gain. There are 10 selectable sample rates from 500 samples/second to 1/3 Mega samples/second. Due to the high sampling rate, this waveform recorder has 2k or 32k/channel on board memory (2048 or 32,768 words). A voltage signal generated from the plasma experiment firing circuitry externally triggers the waveform recorder. This allows the waveform recorder to precisely capture the signals from the phase comparators. Each data signal is stored in its own memory after it is sampled and digitized. One data record at a time will be transferred through the IEEE-488 bus (Metrabyte, Model IE-488) to a computer (DELL Computer Corp, System 316SX).

The DELL system 316SX delivers 386/16MHz performance and runs advanced 32-bit software designed for Intel 80386-based microprocessors. The unit purchased comes with 1MB or RAM memory, 40M-29ms hard disk drive, less than one wait state, color VGA screen with a resolution of 480 x 600 pixels and 16-bit video adapter, an Intel 16MHz 80387 math co-processor, one 5.25" high density (1.2ME) and one 3.5" high density (1.44MB) floppy diskette drives, 1 parallel and 2 serial ports, 6 (full-size) 16-bit and 2 (1 full-size, 1 half-size) 8-bit expansion slots, enhanced 101-keyboard, 200-watt power supply and MS DOS Version 3.3 operating system. In order to transfer data through IEEE bus, a computer program is written in the Asyst software (Keithley, Asyst 3.0 Scientific Software) to communicate with the waveform recorder.

ASYST 3.0 is an integrated software system designed for scientific and engineering aplications. ASYST 3.0 offers sophisticated analysis, graphics, data acquisition and instrument control via Analog-to-Digital, Digital-to-Analog and RS-232 and GPIB/IEEE-488 instrument interfaces. All the ASYST capabilities are accessed and/or modified through English-based commands. This software is capable of doing the following: a) Basic math (complete arithmetic operations, including all trigonometric functions, exponation and logarithms), b) can handle single and double precision integer, real and complex data type numbers, c) it interfaces to Microsoft C (version5) and Fortran (version4.1), d) its waveform processing capabilities include: waveform arithmetic, Fast Fourier Transform (FFT), Inverse FFT, 2D-FFT, I2D-FFT, smoothing, clipping, convolution,etc.

The waveform recorder can function as a talker or listener on the IEEE bus, allowing it to accept controller commands from the computer and to transmit the digital waveform data stored in the waveform recorder memory. As a demonstration, a sine wave input generated by a function generator was successfully captured by the waveform recorder and then transferred to the computer. When the 2k of digital data are transmitted through the IEEE bus to the buffer of the computer, dimension of the buffer array is only half of the original binary file.

2.4 Reduction of Chordal Line Density to Radial Variation of Electron Density

The interferometer described above is designed to measure electron line density along chords of the cylindrically symmetric plasma. The technique of Abel inversion allows the determination of N(r) from Ne (x) length along the chord[12].

For a cylindrically symmetric quantity (such as refractive index) f(r) of which the accessible measurments are chord integrals,

$$F(y) = \int_{-\sqrt{(a^2-y^2)}}^{+\sqrt{(a^2-y^2)}} f(r)\, dy$$

As shown in Fig.4, we may change the x integral into r integral to get

$$F(y) = 2\int_y^a f(r) \frac{r dr}{\sqrt{r^2-y^2}}$$

This relationship between F and f is an integral equation for F. The inverse transform relates the quantity we seek [f(r)] to an integral of F, as follows:

$$f(r) = \frac{1}{\pi}\int_r^a \left(\frac{dF}{dy}\right) \frac{dy}{\sqrt{y^2-r^2}}$$

Note that in the inverse transform, it is the spatial derivative of F (dF/dy) that appears. This tends to make the Abel inversion [f(r)] rather sensitive to any errors in F(y). This will require more channels of chordal measurements to generate accurate spatial derivative of F.

REFERENCES

1. York, T.M, Zakrzwski, C., and Soulas, G., "Diagnostics and Performance of a 1/4-scale MPD Thruster", AIAA 90-2665, July 1990.

2. Zakrzwski, C., " Experimental Investigation Of 1/4-Scale Magnetoplasmadynamic Thruster Without Applied Magnetic Fields and With Applied Magnetic Fields", M.S. thesis, Ohio State University, Columbus, Ohio, 1990.

3. Soulas, G., "Applied Magnetic Nozzle Effects on a Scaled Magnetoplasma dynamic Thruster", M.S. thesis, Ohio State University, Columbus, Ohio, March 91.

4. Veglia, V.P., "The design of Magnetic Mirrors For A Linear Theta Pinch", Scientific Report 81-1, The Pennsylvania State University, University Park, Pennsylvania, January 81.

5. BELL, F.W., HALL GENERATORS CATALOG, Orlando, Florida, 1991.

6. Sugwara, M., "Electron Probe current in a Magnetized Plasma", The Physics of Fluids, Vol. 9(4), April 1966, p.p. 797-800.

7. Chen, F.F., Introduction to Plasma Physics and Controlled Fusion, Plenum Press, New York, 1984.

8. Chang, P.M., Talbot, L., and Touryan, K.J., Electic Probes in Stationary and Flowing Plasmas : Theory and Application, Springervelag New York, Inc., New York, 1975.

9. A. R. Jacobson, "Eight-Cord CO_2 Interferometer for Plasma Density Measurements on ZT-40," SPIE Vol. 288, 1981.

10. W. Demtröder, "Laser Spectroscopy," Springer-Verlag, New York, 1982.

11. I. H. Hutchinson, "Principles of Plasma Diagnostics," Cambridge University Press, New York, 1982.

12. Barr, W. L., "Method for Computing the Radial Distribution of Emittors in a Cylindrical Source." J. Opt. SDC. Am 52, 8, 885 (1962).

Financial Section

FACULTY AND STAFF PARTICIPATION
(BY FUNDING)

T. M. York	Principal Investigator	% Effort	Project Charge
	March 15, 19-Aug. 31, 92	20%	0%
H. Kamhawi	Graduate Research Asso.		
	June. 91-Jan. 92	50%	50%
	Jan. 92-Aug. 92	50%	15%
Ke-I Li	Graduate Research Asso.		
	June 91-Jan. 92	50%	50%
	Jan. 92-Aug. 92	50%	15%

Equipment Procurement and Charges

Magnetic Nozzle Electrical Switch (100-1000A for 500μs-1sec)	$8,809.00
Half-Wave Plate for Beam Rotation	$2,400.00
Data Acquisition Computer (Mother board) repair	$750.00
	$11,959.00